POLITECNICO DI TORINO
Repository ISTITUZIONALE

Experimental results and strength model identification of pure iridium

(Article begins on next page)

04 August 2020

Accepted Manuscript

Experimental Results And Strength Model Identification Of Pure Iridium

Martina Scapin , Lorenzo Peroni , Claudio Torregrosa , Antonio Perillo-Marcone , Marco Calviani , Laura Gomez Pereira , Floriane Léaux , Mickaël Meyer

Please cite this article as: Martina Scapin , Lorenzo Peroni , Claudio Torregrosa , Antonio Perillo-Marcone , Marco Calviani , Laura Gomez Pereira , Floriane Léaux , Mickaël Meyer , Experimental Results And Strength Model Identification Of Pure Iridium, *International Journal of Impact Engineering* (2017), doi: 10.1016/j.ijimpeng.2017.03.019

Highlights

- Mechanical characterization of pure iridium

- Tension tests at different temperatures and strain-rates

- Fracture surface analysis

- Johnson-Cook model identification

- Recrystallization temperature

EXPERIMENTAL RESULTS AND STRENGTH MODEL IDENTIFICATION OF PURE IRIDIUM

Martina Scapin [a], Lorenzo Peroni [a], Claudio Torregrosa[b], Antonio Perillo-Marcone[b],

Marco Calviani[b], Laura Gomez Pereira [b], Floriane Léaux [b], Mickaël Meyer [b]

[a] Department of Mechanical and Aerospace Engineering, Politecnico di Torino, Corso Duca degli Abruzzi, 24 – 10129 Turin, Italy

[b] European Organization for Nuclear Research (CERN) – 1217 Geneva, Switzerland

Abstract

Intense and high energy proton beams are impacted with fixed materials (targets) in order to produce new particles and secondary beams at CERN. In some of these targets, the requirement of reaching high yield production of secondary particles points out to the use of high density materials. The interaction of the beam with the atoms and nuclei of these materials produce extremely fast depositions of energy, highly soliciting them from thermo-structural point of view due to subsequent rise of temperature and pressure waves. Iridium is a good candidate material since exhibits very high density, high melting point, good strength and stability at high temperature, and resistance to thermal shock.

The main goal of this study is the investigation of the mechanical behaviour at different temperatures and strain-rates in tensile loading condition of pure iridium. A series of tests at room temperature at different strain-rates (from 10^{-3} s^{-1} up to 10^4 s^{-1}) was performed in order to obtain information about strain and strain-rate sensitivity of the material. In addition, a series of tests at different temperatures in both quasi-static and high strain-rate loading conditions was performed in order to obtain information about the thermal softening of the material (from room temperature up to 1250 °C). The experimental data were used to identify a strength model able to predict the material behaviour over wide ranges of variation of the variables of interest.

1. Introduction

Iridium is a very rare metal belonging to the platinum group, which possesses a unique combination of properties such as very high density (it is the second densest element after osmium with a density of 22.46 g/cc), high melting point, excellent oxidation and corrosion resistance, and high strength even at high temperature [1-3]. Due to its properties and despite its elevated price, iridium found several applications as structural material in the high technology and nuclear field such as material for the nozzles of rockets or capsules for radioisotope heat sources in spacecraft among others [4-5]. In addition, iridium has found application in the particle accelerators field, in particular as target material of the CERN's Antiproton Decelerator Target (AD-Target) for the production of new particles and secondary beams. Since a very compact target is necessary, a very high dense material has to be used: the core of the current AD-Target design used since 1987 consists on a thin rod of iridium, 3 mm diameter 55 mm length [6]. During operation, this core material is impacted by intense 26 GeV primary proton beams from the CERN Proton Synchrotron perpendicularly to one base (the beam axis is coaxial with the iridium rod). The interaction with the beam produces extremely fast depositions of energy in its interior with a subsequent rise of pressure and temperature, with shock waves generation [7-8]. The pressure distribution assumes an axisymmetric profile around the beam axis and a Gaussian-like profile longitudinally [8]. The pressure provokes the bulge of the material and radial cracks are developed due to high Hoop strains. Moreover, the pressure gradients induces plasticity, which develops in high temperature and high strain-rate conditions. An example of damage induced in the material is reported in Fig. 1 [7, 9].

Fig. 1: Damage induced in Iridium rod as a consequence of high energy proton beam impact (the beam is coaxial with the rod and hits the rod at the centre of one base) during the HRMT27 experiment, in which equivalent conditions as the ones reached in the AD-target core were recreated [7, 9].

With the aim of understanding these complex phenomena numerical simulations represent an extremely useful tool, but the accuracy of the results depends on the use of proper material strength models which can accurately predict the material behaviour beyond yielding at the high temperatures and strain-rates. For these reasons, the main objective of this work is the calibration of the parameters for the Johnson-Cook

model starting from the data coming from a testing campaign which was performed in tension on pure iridium at different temperatures in both static and high dynamic loading conditions.

The material analysed in the present paper was supplied by Goodfellow in form of 4 mm diameter rod. The material is declared to be 99% purity polycrystalline iridium, produced from a drip melted ingot by Electron Beam melting, forged and swaged into a rod. The material is considered as free of elements judged as dangerous contaminants such as C, O, N, H and Re [1-2]. The concentration of others impurities is given in Table 1.
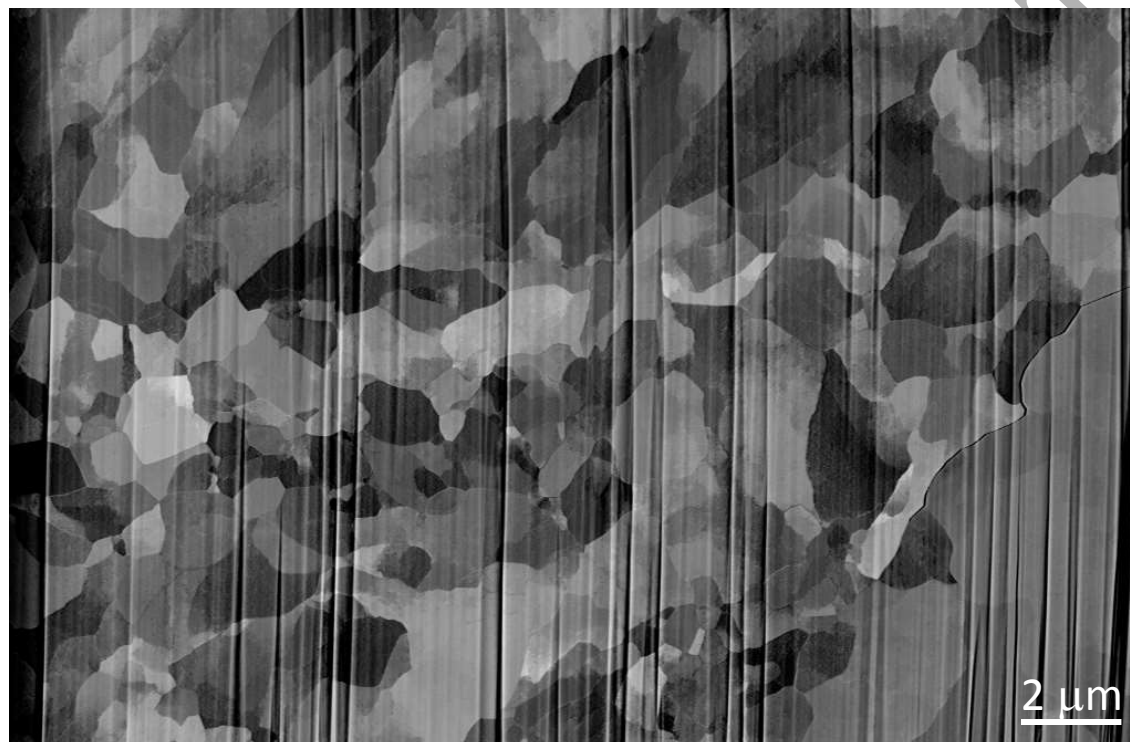
Fig. 2 Microstructure observation on pristine iridium sample.

Table 1 – Concentration of impurities in iridium samples in p.p.m.

Al, Ca, Mo	Fe	Li	Si	Ru	Pd	Pt	W
6	3	7	2	115	15	80	554

No more information was available hence a preliminary investigation of the microstructure was performed by SEM analysis, as reported in Fig. 2, from which it was possible to conclude that the microstructure is heterogeneous, the grain size is in the order of magnitude of some microns and some cracks were present.

2. Bibliographic review

Due to its rareness, elevated price and restricted applications, only few previous studies of mechanical stress-strain properties of pure iridium have been found in the literature. The tensile properties in static conditions ($5 \cdot 10^{-3}$ s^{-1}) and up to 2000 ºC where studied in [10]. This study showed a considerably increase of iridium ductility at high temperatures, from a yield strength (at 0.1% strain) of 990 MPa at room temperature down to 40 MPa at 1600 ºC with a sharp transition around 800 °C. In the same way, the observed elongation to failure varied from 1.1% at room temperature up to 10.2% at 1500 ºC. Iridium, unlike most of others Face-Centered-Cubic (FCC) metals, exhibited a brittle-ductile transition and only moderate ductility at high temperatures. Different modes of fracture were observed: at low temperatures the observed fracture was brittle intergranular fracture (BIF); from 900ºC to 1600ºC the metal became increasingly ductile and failure was partially intergranular and partially transgranular (BTF), probably due to recrystallization processes; above 1600ºC the fracture observed was again entirely intergranular. The brittleness of iridium at low temperature (in comparison to the rest of FCC metals) was studied more in detail in [11], suggesting that below 1000ºC iridium fails intrinsically by BIF. This is, however, a matter of discussion in the literature. Further studies on iridium, e.g. [12-14], were performed on fracture mode (intergranular and transgranular) and on its relation to impurity content. The comparison with the results from tests performed on iridium single crystals suggest that BTF is the inherent fracture mode of polycrystalline iridium, while BIF in iridium may be considered as an impurity-induced fracture mode.

Concerning the dynamic regime, not a single study of the dynamic response of pure iridium has been found in the literature apart from a few publications on stress-strain properties under dynamic and impact loading of DOP-26 (an iridium alloy containing 0.3 % of W to aid fabrication and approximately 40 ppm of Th to improve grain boundary cohesion at high temperatures), mainly motivated by the use of this material as cladding for radioisotope thermo-electric generator [15-16]. More recent publications have been found in the literature on the dynamic testing of DOP-26 alloy in tension [17-18] and compression [19] at different temperatures. In [18], an approach similar to those here proposed was applied to investigate the mechanical behaviour of the iridium alloy DOP-26 between 10^3 s^{-1} and 3×10^3 s^{-1} at high temperature (between 750 °C and 1030 °C). The high strain-rate loading conditions were obtained by using a direct-tension Kolsky bar. These studies revealed that the stress–strain response of the iridium alloy shows significant sensitivity to both strain rate and temperature.

Nevertheless, even if the cited studies can give a broad idea of the response of iridium in dynamic and high temperature regimes, all the dynamic works found were performed in DOP-26 alloy and not pure iridium: the mechanical behaviour of DOP-26 can be significantly different due to influence of this Th precipitates in the grain boundaries. The different mechanical response was confirmed by the results reported in the next section.

3. Experimental procedure

As anticipated in previous paragraphs, the mechanical characterization of pure iridium was performed in tension at different temperatures and strain-rates on dog-bone specimens. A series of tests at room temperature at different strain-rates was performed in order to obtain information about strain and strain-rate sensitivities of the material. The strain-rate sensitivity was investigated starting from 10^{-3} s^{-1} up to 10^3

s[-1]. The medium-low strain-rate tests were performed using electro-mechanical testing machine. The high strain-rate condition was reached by mean of Kolsky Bar setups in direct configuration (see Figures 3 and 4). In addition, a series of tests at different temperatures, in both quasi-static and high strain-rate loading conditions, was performed in order to obtain information about the thermal softening of the material. The investigated range was from room temperature up to 1250 °C. Both for quasi-static and high dynamic loading conditions, the specimen was heated using an induction coil system, controlled with a feedback on the temperature measurement obtained using thermocouples directly welded on the specimen surface. A more exhaustive description of the setups can be found in [20-22], but for this test campaign the improvement was represented by the use of a different solenoid, which was properly designed to allow having optical access to the specimens. A picture of a specimen mounted on the setups used for tests at 10[3] is reported in Figure 3.a, from which it is possible to see the solenoid, which was the same used also for quasi-static tests. The optical access to the specimen gave the possibility to record the video of each test, in order to obtain the information about the deformation history. The tests at low strain-rate were recorded by using a high resolution camera (Pixelink), with a framerate of 2 fps at a resolution of 2592×920 pixels. For the tests at high strain-rate a high speed camera was used (Photron SA5): tests were recorded at 100000 fps with a resolution of 512×128 pixels. For this setup, the signal on the input bar is used as trigger for switching-off of the induction system and switching-on (with a programmable delay) of the high speed camera and lighting system. The video data are used to measure the specimen gage length history, to evaluate the deformed shape and the failure mode of the specimen and finally, to check the applied velocity and the specimen equilibrium.
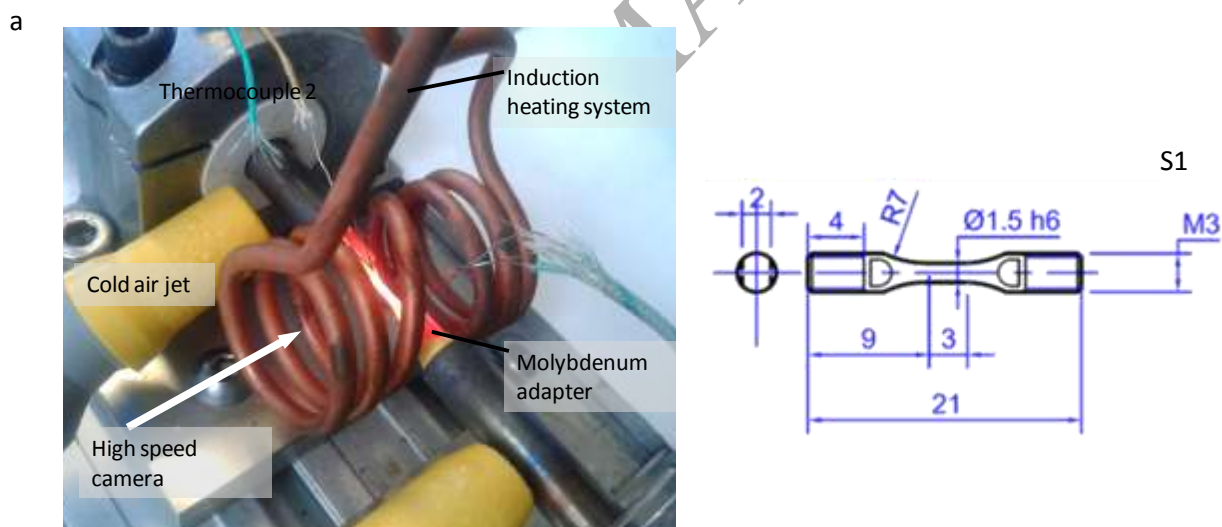
a

Fig. 3.

Detailed picture of the experimental setup used for tests at high temperatures at 10[3] s^{-1} (a); sketch of the specimens S1 used for the testing campaign (b).

For the testing campaign, dog-bone specimens (labelled S1) with gage length of 3 mm and gage diameter of 1.5 mm were used. As anticipated in the introduction, pure iridium is a rare and highly expensive material, hence the dimension of the specimens was comparable to the size of the real component [7] and the number of available samples was limited to 25.

After testing, fracture surfaces were examined with the help of the digital microscope KEYENCE VHX 1000 and the scanning electron microscope (SEM) field emission gun FEG Sigma (ZEISS), with the Everhart-Thornley Secondary Electron (SE2) and back-scattered electron (AsB) detectors.
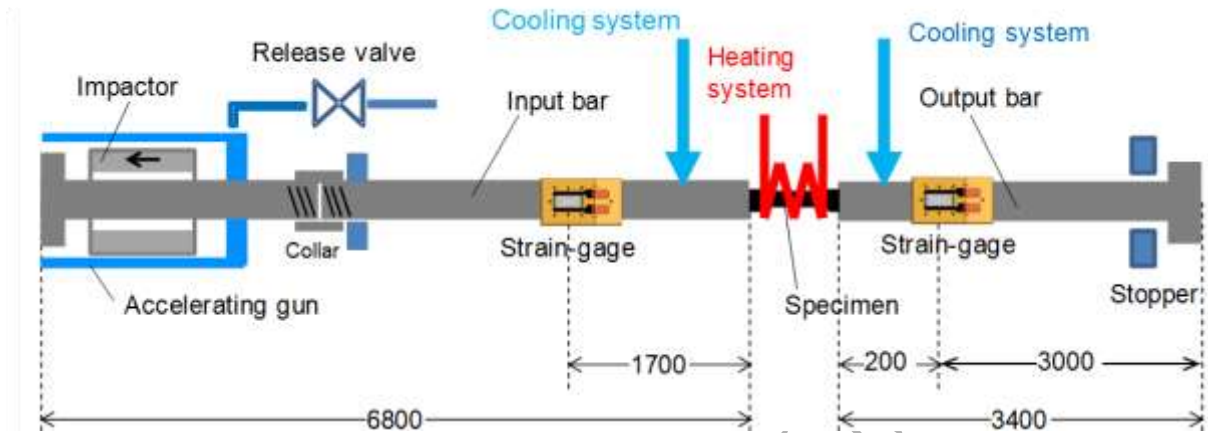

Fig. 4.

Schematic representation of the experimental setup used for tests at 10^3 s^{-1}.

4. Experimental results

Due to the limited number of specimens, it was not possible to evaluate the data scatter for all the loading conditions. In order to validate the obtained results in the investigated range of temperature, a lot of intermediate temperatures (between room temperature and 1250°C) were investigated: from a statistical point of view, this allows controlling the reliability of each result (instead of performing a certain number of repetitions of the same loading condition). Nevertheless, in some cases, more than one test was performed.
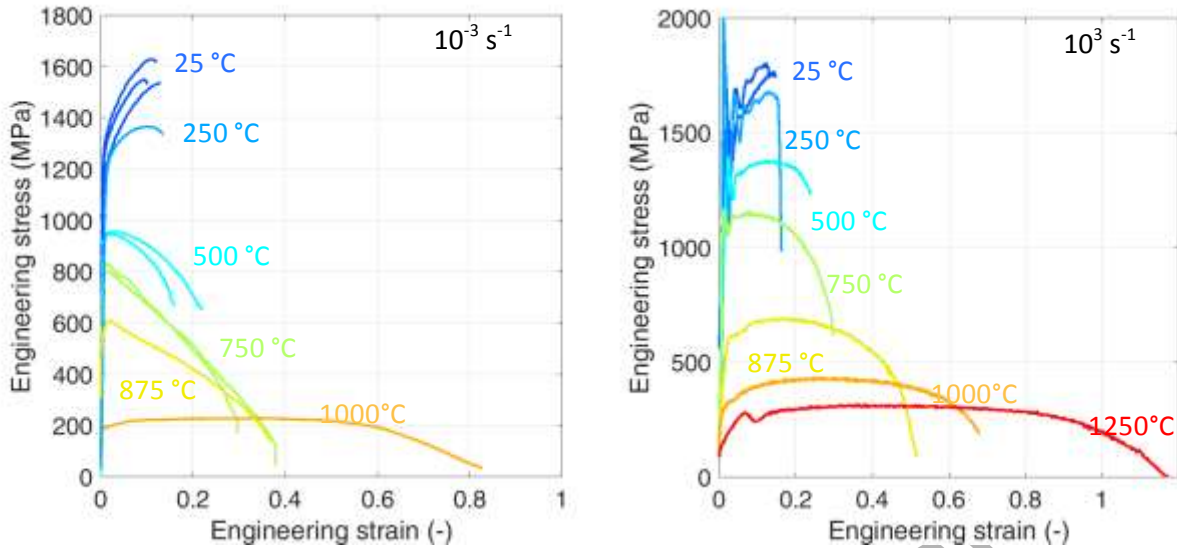
Fig. 5.

Experimental results – engineering stress vs. engineering strain curves at different strain-rates and temperatures.

For all the tests, the load applied by the testing equipment and the deformation of the specimen, measured from the videos, were managed and starting from these data, the engineering stress vs. engineering strain curves were obtained as reported in Figure 5. The deformation of the specimen was directly measured on the video by following the displacement of some points on the surface and using digital images elaboration techniques: this allowed to obtain a more precise evaluation of the deformation avoiding correction introduced by clearance, deformation of specimen outside the gage length and machine compliance. In Hopkinson bar tests, the strain-gage signals were used to determine the force; the deformation measurements coming from video elaboration and strain-gages signals were compared for a crosscheck.

The last frames extracted from the recorded videos are reported in Figure 6 for both quasi-static and dynamic tests at different temperatures. In Figure 7, the sequence of the dynamic test at 1250 °C is shown.
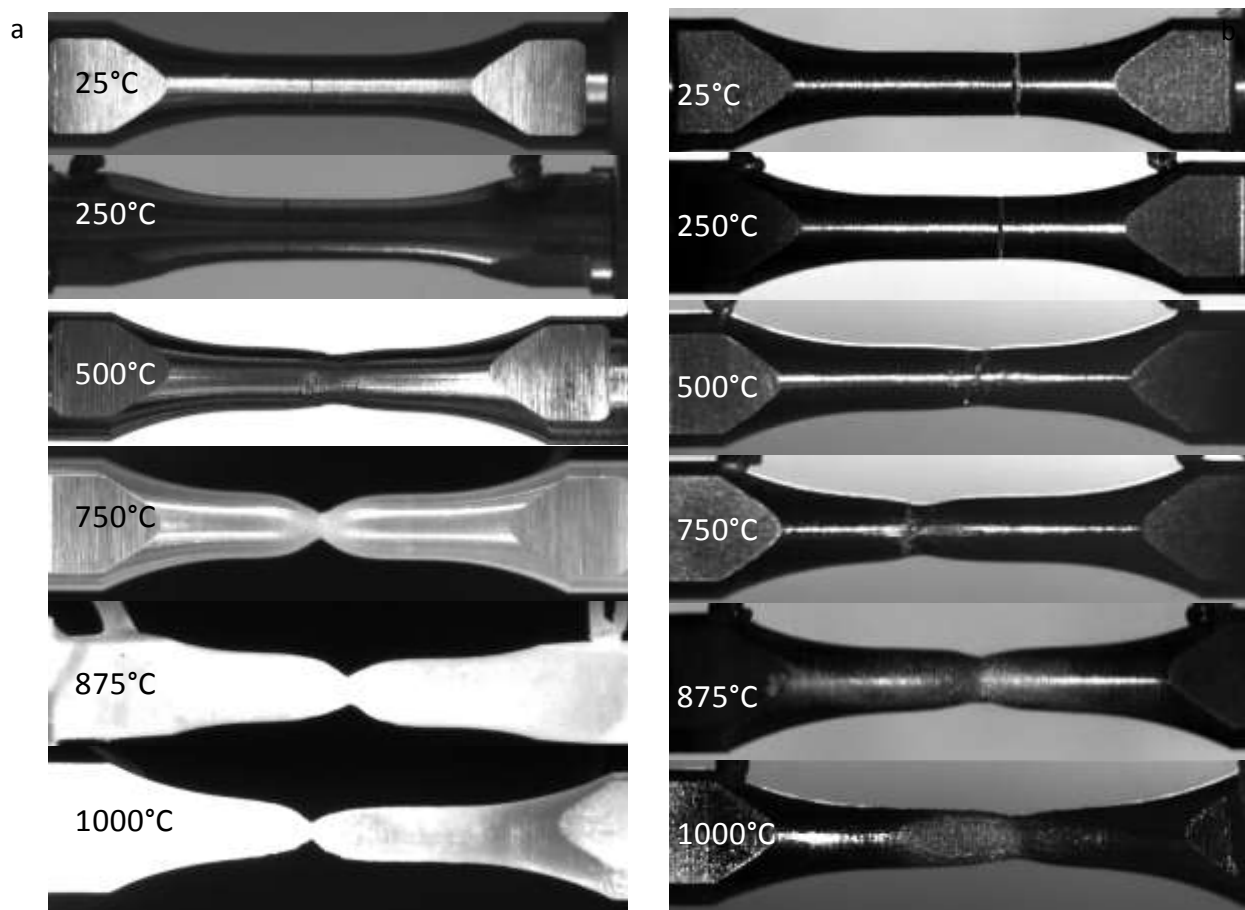
Fig. 6.

Experimental results – last frames extracted from recorded videos of tests at different temperatures: quasi-static tests (a); dynamic tests nominally at $10^3\,s^{-1}$ (b).

From the results it is possible to notice that the material is sensitive to both strain-rate and temperature, but it exhibits a different behaviour as a function of temperature at low and high strain-rates. A more detailed analysis in this sense is presented in paragraphs 4.1-4.4.
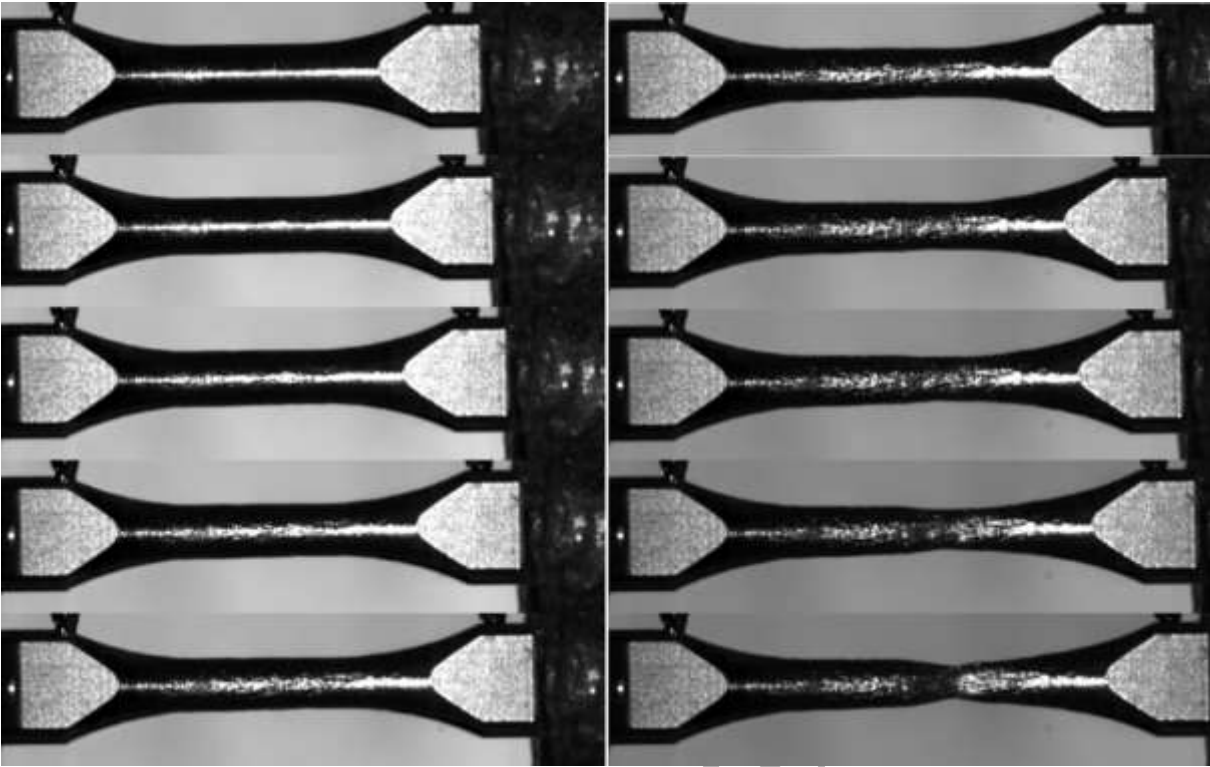
Fig. 7.

Sequence of frame extracted from the video recorded for the test at 10^3 s^{-1} of strain-rate and 1250 °C of temperature (the time interval between the reported images is 50 μs).

4.1 Low temperatures for quasi-static and dynamic regimes.

Both in quasi-static and dynamic regimes, the mechanical behaviour at low temperature is characterized by a uniform elongation phase, followed by a brittle fracture, as confirmed by the microscopic observations of the fracture surfaces presented in Figures 8.a and 8.b. The fracture surface displays the typical elements of BTF [23-25]: classic cleavage with river patterns, cracked grain boundaries and several cleavage steps.
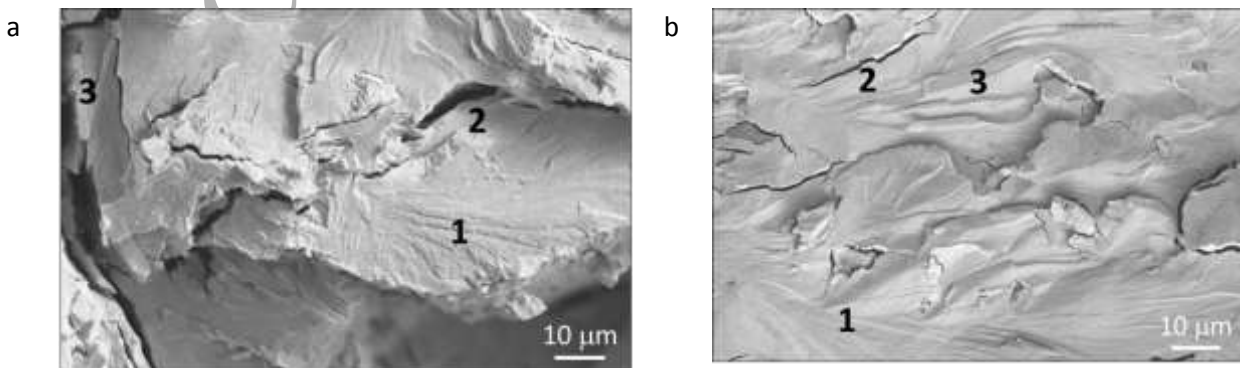

Fig. 8.

SEM images (secondary electrons): Fracture surfaces at 25°C: a) in quasi-static and b) in dynamic regimes. The images show: classic cleavage with river patterns (e.g. 1), cracked grain boundaries (e.g. 2) and several cleavage steps (e.g. 3).

4.2 Medium temperatures for quasi-static and dynamic regimes.

Between 250°C and 850°C, at low strain-rate, the mechanical response shows an early localized necking with a limited or absent hardening phase. Under these loading conditions, a radical change of the fracture behaviour starts to be visible. At 500°C, the fracture mode of the material corresponds still mainly to BTF (Figure 9.a), while at 750°C, the surface displays a mixed brittle fracture mode: BTF accompanied with a considerable portion of BIF (Figure 9.b) [12, 24].

On the contrary, by increasing the strain-rate, the material shows uniform elongation and hardening before necking. At 500°C the fracture mode continues to be pure BTF (Figure 10.a), at 750°C the presence of BIF starts to appear in the surface (Figure 10.b). However, in this case, the ratio between BTF and BIF regions is about 7:1.
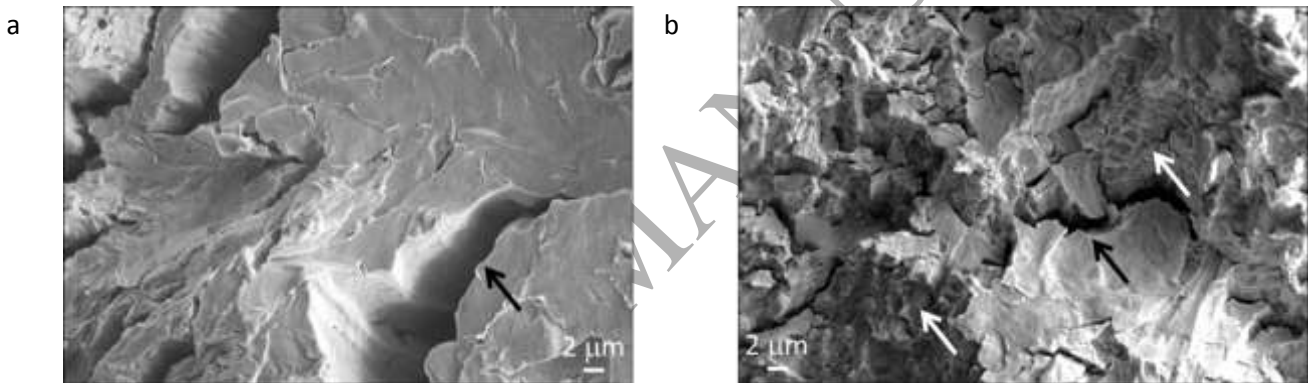
a

b

Fig. 9.

SEM images (secondary electrons): Fracture surfaces at 500°C (a) corresponding mainly to BTF (black arrow), and 750°C (b), in quasi-static regime mixed fracture mode BTF-BIF (black and white arrows, respectively) is visible.
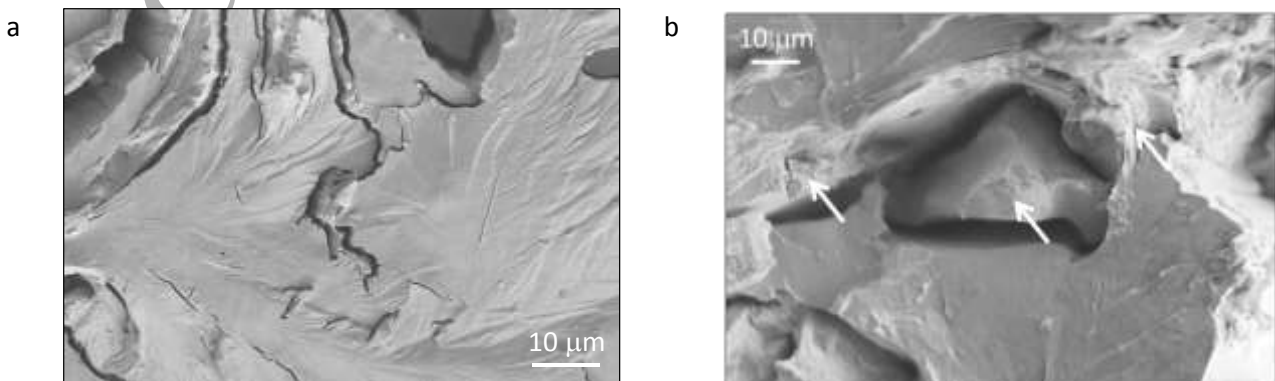
a

b

Fig. 10.

SEM images (secondary electrons): Fracture surfaces at 500°C (a) showing a pure BTF fracture and 750°C (b), in dynamic regime), where in addition to BFT, presence of BIF is visible (white arrows).

4.3 At high temperature for quasi-static and high strain rates.

By increasing the temperature (over 1000 °C), independently from the strain-rate, uniform elongation with necking was present and material was practically behaving the same way (Figure 3). As shown in Figure 11.a, at 1000°C and in static regime, the BIF ratio increases, to reaching the 75-80%. At 1000°C and high strain rates, the mixed (BTF and BIF) brittle fracture remains but BTF is still predominant (Figure 11.b).
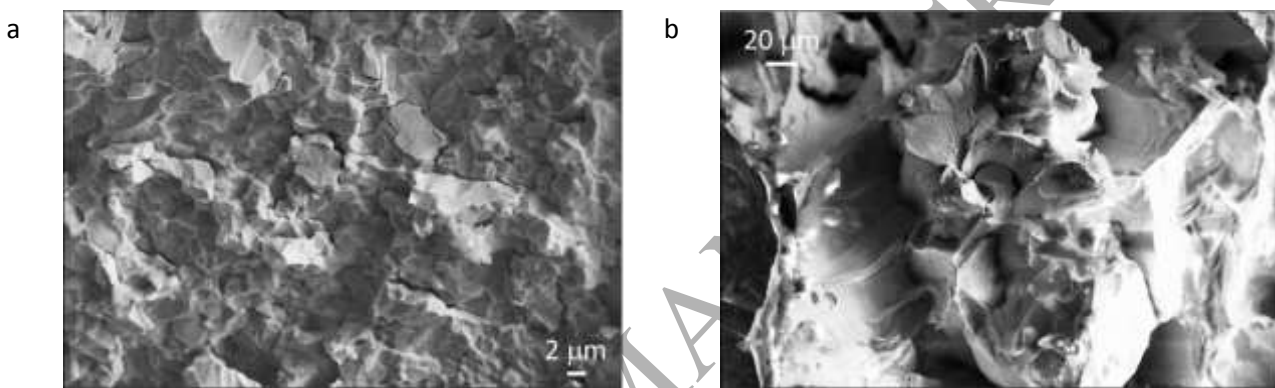
a

b

Fig. 11.

SEM images (secondary electrons): fracture surfaces at 1000°C, in quasi-static (a) regime, where BIF reaches 75-80% of the fracture surface, while in dynamic regimes (b) BTF mode remains predominant.

4.4 Influence of the strain rate

While at high strain-rates, BTF stays predominant whatever the temperature, in quasi static conditions, a clear transition is observed from a mainly BTF fracture surface to a mainly BIF fracture surface. This change of behaviour is linked to the recrystallization phenomenon, observed in Figure 12.a, taking place in a large extend in static conditions. From the bibliography, recrystallization is expected to occur around 1000°C [13, 24]. The recrystallization leads to a modification in the fracture mode of the material, from BTF to a mixture of BIF and BTF [14]. At high strain-rate the BTF mode stays predominant since the recrystallization reached a less advanced stage than in quasi-static mode where the material stays longer at high temperature.
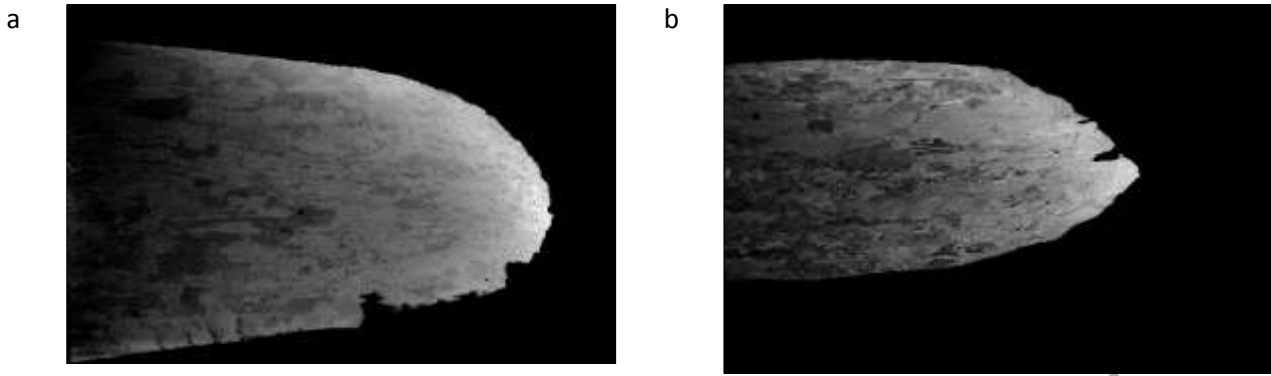
Fig. 12.

SEM images (backscattered electrons): Fracture surfaces at 1000°C, in quasi-static (a) and dynamic (b) regimes: the recrystallization is more advanced in the quasi-static tested specimen than in the dynamically tested one.

4.5 Strain to failure

In order to estimate the strain at failure, for each specimen, the post-mortem diameter (*d*), measured from SEM frontal images of the fracture surface, was used to estimate the strain at fracture by the relation:

$$\varepsilon_f = 2\ln\frac{d_0}{d}$$

(1)

where d_0 is the initial diameter of the gage section. In Figure 13, the calculated strains at failure vs. temperature are reported: the data obtained in quasi-static and dynamic loading conditions are compared. As it is possible to notice, the strain at failure is independent from the strain-rate, even if, the data scatter seems to be lower at high strain-rate. The data were interpolated with a linear model, in accordance with a simplified formulation of the Johnson-Cook fracture model [26], which expresses the strain at failure as follows:

$$\varepsilon_f = D_1\left(1 - D_5\frac{T - T_r}{T_m - T_r}\right)$$

(2)

Where T_r is 298 K and T_m is 2683 K. The coefficient obtained are D_1=0.1 and D_5=-26.09 (D_1 is the average value of strain at fracture obtained from the tests at 25 °C).

The SEM pictures of the fracture surfaces are reported for some loading conditions in Figures 14 and 15.
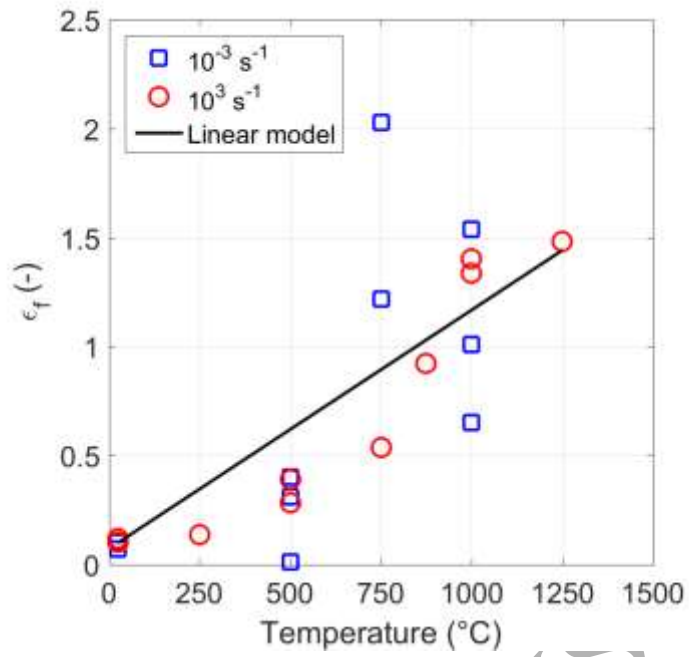
Fig. 13.

Strain at failure obtained from the post-mortem measurements of the diameter: data fit with a linear model as a function of temperature.
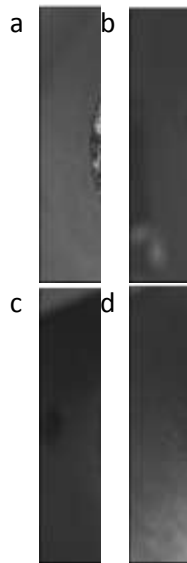

Fig. 14.

SEM frontal images of the fracture surface for tests in quasi-static regime at 25°C (a), 500°C (b), 750°C (c) and 1000°C (d).
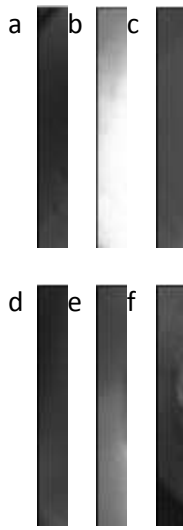

Fig. 15.

SEM frontal images of the fracture surface for tests at high strain-rate regime at 25°C (a), 500°C (b), 750°C (c) 875°C (d), 1000°C (e) and 1250°C (f).

5. Data analysis

The aim of this work is to get suitable strength model(s) able to reproduce the experimental behaviour of the material over the entire investigated ranges of temperature and strain-rate in terms of flow stress description. Some preliminary considerations have to be done.

In Fig. 16, the ultimate strength as a function of temperature obtained from the testing campaign was reported and compared with the data available from scientific literature for pure iridium in quasi-static loading condition and DOP-26 both in quasi-static and dynamic regimes. By comparing the data, it is possible to conclude that the material tested in [10] has a different microstructure, which is responsible of a lower material strength at low temperature with a less pronounced transition; obviously after recrystallization, the ultimate stress values are more comparable for the two materials. The comparison with DOP-26 data reveals that the alloy shows a lower strength as well as a different thermal softening behaviour, hence it is not possible to use these data to predict or deduce the pure iridium behaviour.
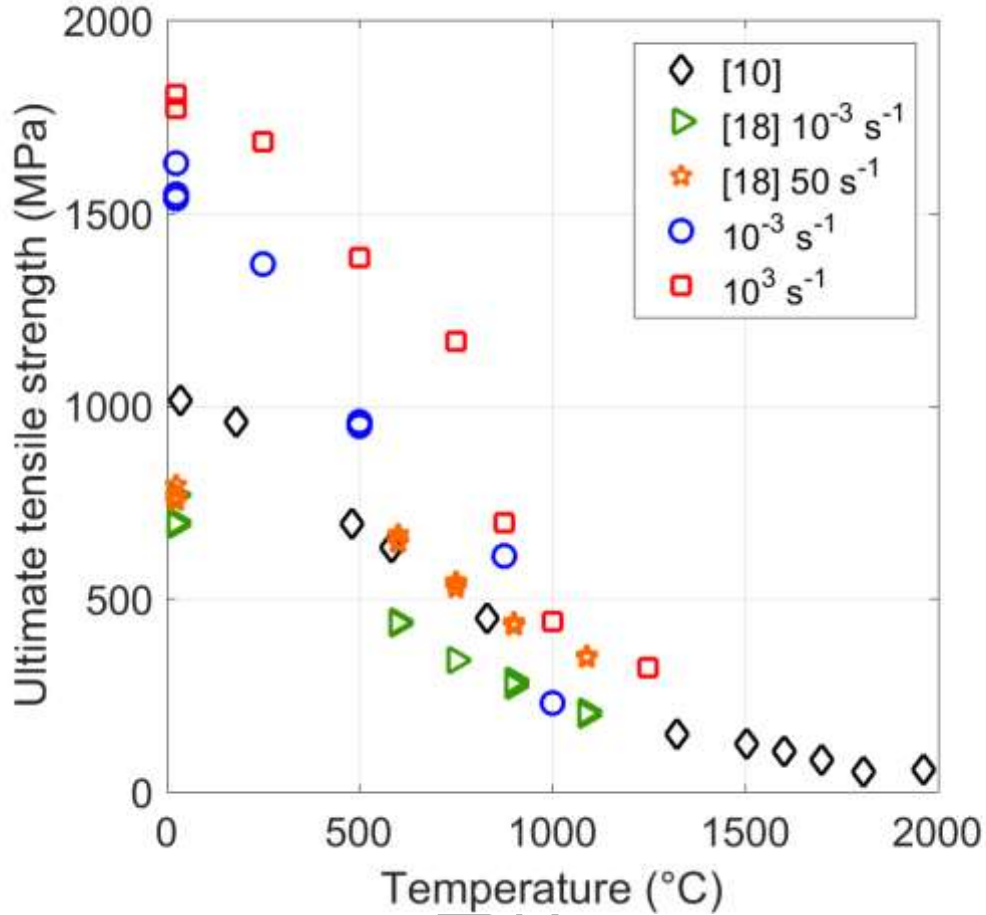
Fig. 16.

Ultimate strength vs. temperature: comparison with data coming from scientific literature.

By looking the results of Figure 5, it is possible to assess that by considering the commonly used material models, such as Johnson-Cook [26] and Zerilli-Armstrong [27-28], as well as more complicated and physically-based models such as Steinberg-Guinan [29] and MTS [30], it will not be possible to describe with a unique model the material behaviour in quasi-static regime between 250 and 875 °C within the other loading conditions: in all the other loading conditions the material shows a significant uniform elongation before fracture or necking, while that range was characterized by early necking. In this perspective, starting from the data expressed in terms of engineering stress-strain curves (quasi-static and dynamic cases), under the hypothesis of uniform stress and volume conservation, the engineering curves were transformed into logarithmic (true) stress vs. effective plastic strain. Obviously, this elaboration is valid until the instability condition is reached. The idea was to use the Johnson-Cook model to fit these data:

$$\sigma = \left(A + B\varepsilon^n\right)\left(1 + C\ln\frac{\dot{\varepsilon}}{\dot{\varepsilon}_0}\right)\left(1 - \left(\frac{T - T_r}{T_m - T_r}\right)^m\right)$$

(3)

in which *A*, *B* and *n* define the hardening part, *C* the strain-rate sensitivity and *m* the thermal softening.

As first step, a preliminary data fit was performed by using an analytical model: in this phase a single case optimization for each loading condition was performed from which it was possible to obtain smoother equivalent stress vs. equivalent plastic strain data (this, for example, eliminates the typical oscillation in the first phase of the Hokinson Bar results). For this purpose, the hardening part of the Johnson-Cook model was used. By plotting the obtained yield stress values as a function of temperature (see the markers in Figure 16), it was possible to notice that the material behaviour can not be adequately described by a unique strength model due to the presence of the sharp transition, which is in accordance with the results found in [10]. For this reason, two different sets of parameters were identified: one (JC1) to be adopted before and the other (JC2) after the transition. On the range 750°C-1000°C the material shows a discontinuity in its mechanical response. This is related with the recrystallization phenomenon explained here above. The adopted procedure is a multi-cases optimization, based on the minimization of the mean square error between predicted and experimental-derived data. In particular, two different optimizations were performed, one for each region of temperature (before and above the recrystallization temperature), in which in the meantime all the corresponding experimental data were considered as target functions: this allowed finding the two sets of parameters that produce the best global comparison. The variables of optimization were *A*, *B*, *n*, T_m and *m* for the JC1 while *A*, *B*, *n* and *m* for the JC2. For temperatures under the recrystallization, the melting temperature was considered a variable of optimization in order to improve the quality of the data fit, while T_m was fixed to the melting temperature of pure iridium in the second range, in order to constrain the material strength to zero at that value. The reference temperature *Tr* was set equal to 25 °C for JC1 and to 875 °C for JC2. In both the ranges, the reference strain-rate was fixed to 0.001 s^{-1}, which corresponds to the minimum strain-rate. The final sets of parameters were reported in Table 2. The models prediction for the yield stress in the two regions is reported in the diagram of Figure 17 and compared with those obtained from the single-case optimization step. As it is possible to notice, the two sets of parameters are able to correctly reproduce the yield stress reduction as a function of temperature. In the diagram of Figure 17, also the model prediction at higher strain-rate (10^4 s^{-1}) is shown, since it will be useful for the analysis presented in the following.
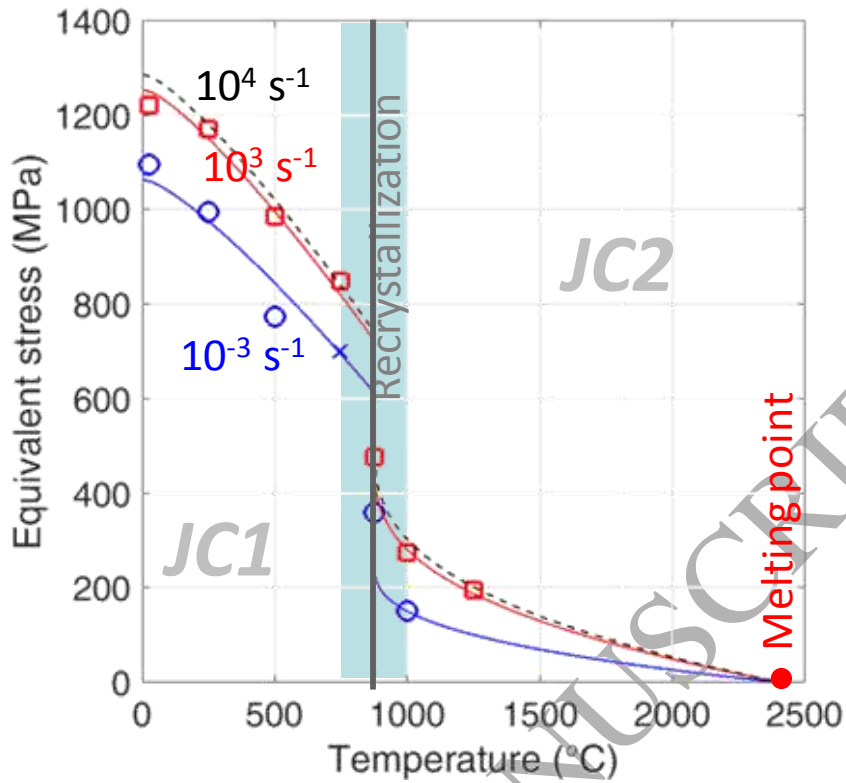
Fig. 17.

Yield stress as a function of temperature: comparison between single-case optimization results (i.e. experimental data) and Johnson-Cook model prediction; identification of the recrystallization temperature

Table 2 - optimized sets of parameters.

Parameter (Units)	JC1	JC2
A (MPa)	1054	247
B (MPa)	1632	499
n (-)	0.401	0.5
C (-)	0.013	0.065
$\dot{\varepsilon}_0$ (s^{-1})	0.001	0.001
T_r (K)	298	1148
T_m (K)	1996	2683
m (-)	1.25	0.357

5.1 Models validation

The obtained sets of parameters were then used in FE simulations which reproduce each loading condition. All the simulations were performed in LS-DYNA with an explicit integration method on a 2D axisymmetric model with sub-integrated elements (one integration point for each element). The boundary conditions

were applied to the specimen ends in terms of velocity profiles. A 2D-remeshing algorithm was applied in order to control the element dimension and get reliable results even if high value of plastic strain was reached during the necking phase.

The models predictions over the entire range of strain are reported in Figure 18 in term of engineering stress vs. engineering strain and compared with the corresponding experimental data. The two sets of parameters were obtained by considering the experimental data up to necking initiation, but the validity of the previsions were checked also in necking regime up to fracture. As expected, the models are able to reproduce the experimental data during uniform elongation with a sufficient level of accuracy for all the loading conditions, except for the cases in which localized necking is present since the end of the elasticity. In dynamic case at 875 °C, the obtained poor quality results can be explained as the unpredictable response of the material within the recrystallization range. Especially at very high temperature, in which the uniform elongation phase is followed by a considerable necking phase, the model previsions are able to reproduce with a sufficient level of accuracy the material responses over the most part of necking.
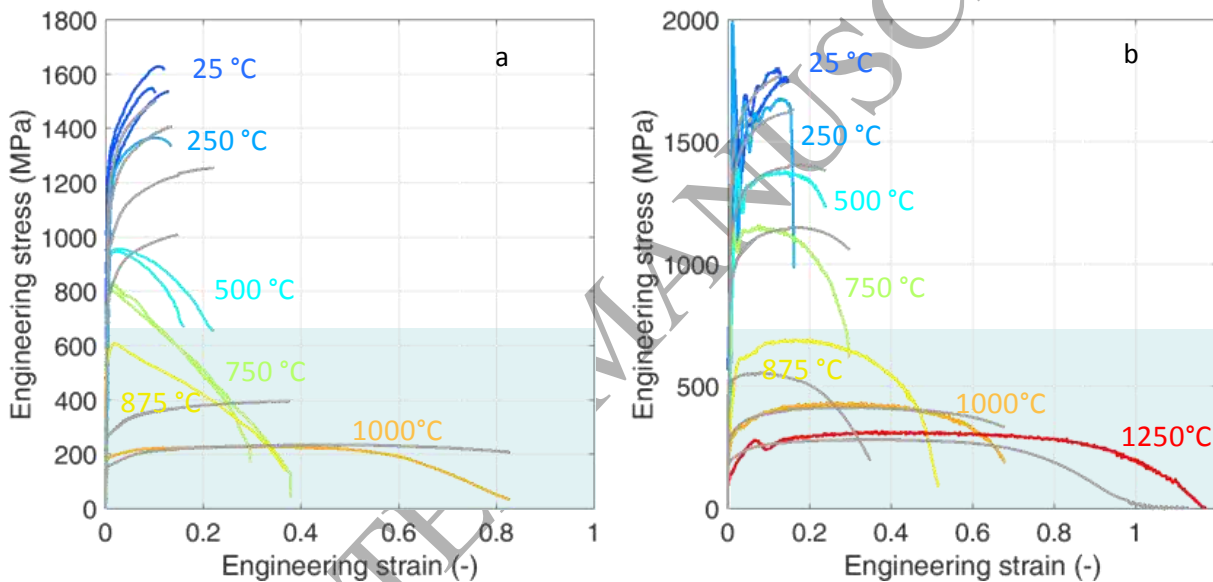

Fig. 18.

Computed (FE simulations) vs. experimental engineering stress-strain data: a) low strain-rate; b) high strain-rate.

A qualitative comparison between experimental and computed deformed shape is reported in Fig. 19, from which it is possible to conclude that the strength model can correctly reproduce the material response also in terms of deformed shape during the necking regime.

Fig. 19.

Comparison of the final deformed shape (before fracture) obtained from computed and experimental results for the test performed at 10^3 s^{-1} of strain-rate and 1000 °C of temperature.

In order complete the models validation and to test their capability to predict the material behaviour also at higher strain-rate, new experimental tests were performed at ultra-high strain-rate about 10^4 s^{-1}. This loading conditions was obtained by using a miniaturized Kolsky setup in direct configuration [21]. In Figure 20, a picture of the specimen mounted in the setup is reported as well as the sketch of the specimen, which is a miniaturized sample (labelled S2) with gage length of 1.5 mm and gage diameter of 1.5 mm (only 7 specimens were available for S2 geometry).
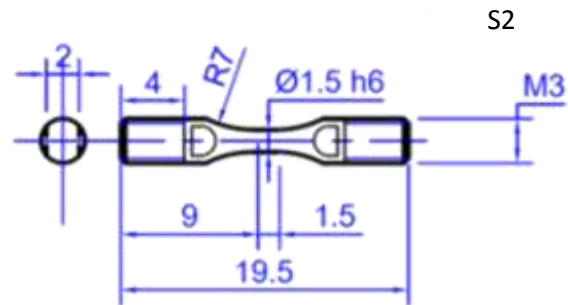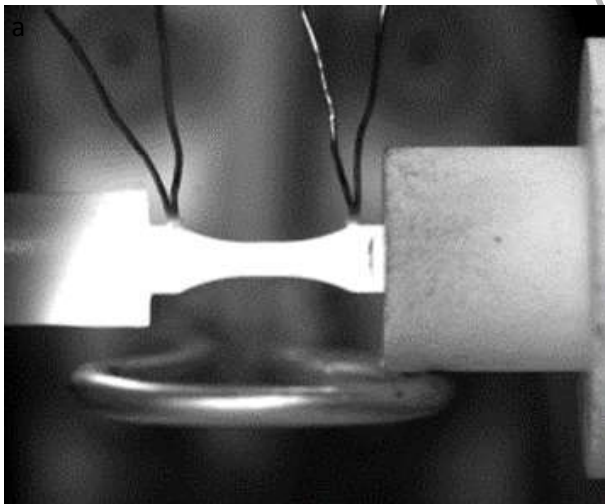

Fig. 20.

Picture of the specimen mounted on the miniaturized Kolsky bar setup for tests at 10^4 s^{-1} (a), sketch of the specimens S2 used for the testing campaign (b).

With respect to the setup described in [21], some important developments were carried out. An induction heating system was coupled also with this setup, allowing to perform tests at high temperature (the maximum temperature reachable was 750 °C, hence only the JC1 model could be validated). With respect to the system used for test on S1 geometry, in this loading condition, a smaller opened solenoid was used and it was placed under the specimens (see Figure 20). The design of the solenoid allowed to keep the

optical access and to record the tests: the high speed camera Photron SA5 was used and the videos were recorded at 300000 fps with a resolution of 320×56 pixels. Another other important improvement came from the video: as a matter of fact, in this loading condition the most (i.e. unique) reliable data on the specimen deformations was obtained from the image analysis. The entire pulse duration is about 100 μs and the input bar is moved at 25-30 m/s in 20 μs, which corresponds to an acceleration greater than 10^5 g. In these conditions, it is impossible to obtain reliable data from any wired measuring system (e.g. strain-gage). Here, the strain-gage signal on the input bar is only used for trigger purpose.
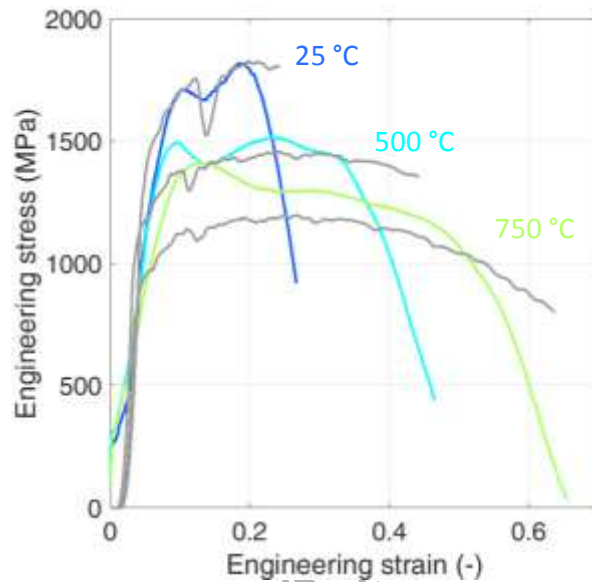
Fig. 21.

Experimental results at 10^4 s^{-1} – engineering stress vs. engineering strain curves at different strain-rates and temperatures and comparison with the corresponding computed (FE simulations) quantities.

In Figure 21, the results of tests performed at different temperatures at ultra-high strain-rate are reported for three different testing conditions in temperature in term of engineering stress vs. strain curves. These data were finally compared with those obtained from the FE simulations of these tests. The comparison is shown in Figure 18 and allowed to conclude that the JC1 model is able to reproduce the material behaviour with a sufficient level of accuracy also at this strain-rate at different temperatures.

6. Conclusions

In this work, the investigation of the mechanical response of pure iridium was performed in tension at different temperatures and strain-rates in order to obtain valuable information for the use of this material in the fixed-target physics programme at CERN, in particular applicable to the antiproton production target. A methodology for testing materials at high and ultra-high strain-rates at various temperatures was applied. The methodology consists of performing dynamic tensile tests using Kolsky Bar setups (standard for tests at 10^3 s^{-1} and miniaturized for tests at 10^4 s^{-1}) coupled with an induction heating system, which is properly design to concentrate the heat flux in the gage length of the specimen. The investigated range in temperature was from room temperature up to 1250 °C. The Improvement of the setups allows the fast

video recording of the tests at high temperature and strain-rates. A post-mortem analysis was performed to evaluate the strain at failure as a function of temperature as well as to identify the mode of fracture. Two microscopic modes of fracture have been observed depending on temperature and strain-rate; at temperatures below 750°C the BTF mode is predominant in both quasi-static and dynamic conditions while above 750°C the observed fracture starts to be mixed BIF and BTF. The higher the temperature the higher BIF to BTF ratio. This change of mode of fracture is attributed to recrystallization processes and grain growth at high temperatures. Regarding the strain-rate influence, it was observed that at high temperature and high strain-rate the BTF is more common than BIF in comparison to quasi-static. This is mainly attributed to the fact that at high strain-rate tests the recrystallization is less developed since the specimens were exposed less time to high temperature.

In addition, the experimental data obtained from quasi-static and dynamic tensile tests are processed in order to get the material model identification. For each loading condition, the logarithmic stress-strain curves were fitted to get equivalent stress-strain curves up to necking initiation. Two different Johnson-Cook models were identified, in order to model the material behaviour at low and high temperature: the material exhibits recrystallization around 800 °C, which is inside the investigated range.

The validity of the obtained models was investigated via FE numerical simulations: a model of each experimental tests was realized and the computed results in terms of macroscopic engineering stress-strain curves were compared with experimental data. Moreover, the capability of the models to extrapolate the material behaviour at different strain-rates was demonstrate by comparing the computed results with experimental ones at 10^4 s^{-1}. Finally, the extracted strength models will be also used in numerical simulations and confronted with experimental data of dynamic response of iridium targets recorded during the HRMT27-Rodtarg experiment at CERN [7-8], which is related to the motivation of this work, i.e, dynamic response of fixed-targets in accelerator technology when impacted by intense high energy proton beams.

Acknowledgments

References

[1]   E. K. Ohriner, *Processing of Iridium and Iridium Alloys,* Platinum Metals Rev., 2008, 52, (3), 186–197.

[2]   N. K. Wahl, Master Thesis: *Natural-convective high-temperature oxidation of iridium*, Montana State University, 1974.

[3]   L.B Hunt, *A History of Iridium*, Platinum Metals Rev., 1987, 31, pp. 32-41

[4]   B. Fischer, A. Behrends, D. Freund, *High Temperature Mechanical Properties of the Platinum Group Metals*, Platinum Metals Rev., 1999, 43, pp 18-28.

[5]   H. Inouye, *Platinum Group Alloy Containers for Radioisotopic Heat Sources*, Platinum Metals Rev., 1979, 23, pp. 100-108.

[6] C. Torregrosa, A. Perillo-Marcone, M. Calviani, *Designs Characteristics and Main Inherent Concerns of the Antiproton Decelerator Target*, CERN-ACC-NOTE-2015-0004, Geneva 2015.

[7] C. Torregrosa, A. Perillo-Marcone, M. Calviani et al., *The HiRadMat 27 experiment: exploring high-density materials response at extreme conditions for antiproton production,* Proceeding of IPAC2016, Busan, Korea, (2016) p. 3705-3708

[8] M. Scapin, L. Peroni, V. Boccone, F. Cerutti, *Effects of High-Energy Intense Multi-Bunches Proton Beam on Materials,* Computers and Structures, 141:74-83, 2013

[9] C. Torregrosa, et al., *CERN antiproton target: hydrocode analysis of its core material dynamic response under proton beam impact*, Phys. Rev. ST Accel. Beams 19, (2016).

[10] B.L. Mordike, C.A. Brookes, *The tensile properties of iridium at high temperatures*, Platinum Metals Rev., 1960, 4, pp 94-99.

[11] S. S. Hecker, D. L. Rohr, D. F. Stein, *Brittle fracture in iridium*, Met. Trans. A, 9A (1978), pp. 481-488

[12] P. Panfilov and A. Yermakov, *Brittle transcrystalline and intercrystalline fracture in polycrystalline fcc metal (iridium)*, TMS 2002 Fall Meeting, October 6-10, 2002, Columbus (OH), US.

[13] P. Panfilov and A. Yermakov, *Brittle Intercrystalline Fracture in Iridium*, Platinum Metals Rev., 2001, 45, 179-183

[14] P. Panfilov, A. Yermakov. *Mechanisms of inherent and impurity-induced brittle intercrystalline fracture in pure FCC-metal iridium*, International Journal of Fracture 128: 147–151, 2004.

[15] T. C. George and M. F Stevens, *High temperature impact properties of DOP-26 iridium*, Los Alamos National Laboratory, Report no, 77980253, (1988)

[16] George, T. G., *High-strain-rate, High-temperature Biaxial Testing of DOP-26 Iridium*, Los Alamos National Laboratory Report, LA-11065, (1988)

[17] J.H. Schneibel, C.A. Carmichael, E.P. George, *High Strain Rate Tensile Testing of DOP-26 Iridium*, Oak Ridge National Laboratory Report, ORNL/TM 2007/81 (2007)

[18] B Song, K. Nelson, H. Jin, R. Lipinski, J. Bignell, *Dynamic High-Temperature Characterization of an Iridium Alloy in Tension*, SANDIA REPORT SAND2015-8380 (2015).

[19] B. Song, K. Nelson, R. Lipinski, J. Bignell, G. Ulrich and E. P. George, *Dynamic High-temperature Testing of an Iridium Alloy in Compression at High-strain Rates*, Strain (2014) 50, 539–546

[20] M. Scapin, *Mechanical characterization and modeling of the heavy tungsten alloy IT180*, INTERNATIONAL JOURNAL OF REFRACTORY METALS & HARD MATERIALS, (2015) vol. 50, pp. 258-268.

[21] Martina Scapin; Lorenzo Peroni; Claudio Fichera; Andrea Cambriani, *Tensile behaviour of t91 steel over a wide range of temperatures and strain-rate up to 10^4 s^-1.* Journal of materials engineering and performance, (2014) vol. 23, pp. 3007-3017.

[22] Scapin M.; Peroni L.; Fichera C., *Mechanical Behavior of Glidcop Al-15 at High Temperature and Strain Rate*, Journal of materials engineering and performance, (2014) vol. 23 n. 5, pp. 1641-1650.

[23] P. Panfilov, *Fracture behaviour of polycrystalline iridium under tension in the temperature range 20-1500°C*, Journal of materials science letters 13 (1994) 137-141.

[24] P. Panfilov, V. Novgorodov and A. Yermakov, *On the inherent fracture mode of iridium at room temperature*, Journal of materials science 40 (2005) 5983–5987.

[25] P. Panfilov and A. Yermakov, *On brittle fracture in polycrystalline iridium*, Journal of materials science 39 (2004) 4543-4552.

[26] G.R. Johnson and W.A. Cook, *Fracture characteristic of three metals subjected to various strains, strain rates, temperatures and pressures* , Engineering fracture Mechanics, (1985) 21(1):31-48.

[27] R.W. Armstrong and F.J. Zerilli, *Dislocation Mechanics Based Analysis of Material Dynamic Behaviour*, J. Phys., (1988) C3–9(49), p 529–534.

[28] Steinberg, D.J.; Cochran, S.G.; Guinan, M.W., *A constitutive model for metals applicable at high-strain rate*, Journal of Applied Physics, (1980) 51 (3): 1498.

[29] Steinberg, D.J.; Lund, C.M., *A constitutive model for strain rates from 10−4 to 106 s−1*, Journal de Physique, (1988) Colloques 49 (3): 3–3, retrieved 2009-05-13.

[30] Follansbee, P.S.; Kocks, U.F., *A constitutive description of the deformation of copper based on the use of the mechanical threshold*, Acta Metallurgica, (1988) 36 (1): 81–93.